Article:
Kudzotsa, I, Phillips, VTJ, Dobbie, S et al. (6 more authors) (2016) Aerosol indirect effects on glaciated clouds. Part I: Model description. Quarterly Journal of the Royal Meteorological Society, 142 (698). pp. 1958-1969. ISSN 0035-9009

https://doi.org/10.1002/qj.2791

Aerosol Indirect Effects on Glaciated Clouds. Part I: Model Description.†

Innocent Kudzotsa*[a], Vaughan. T. J. Phillips [b], Steven Dobbie [c], Marco Formenton [b], Jiming Sun [d], Grant Allen [e], Aaron Bansemer [g], Dominick Spracklen [c], Kirsty Pringle [c],

[a]*Department of Physics, University of Zimbabwe, MP 167 Mt Pleasant, Harare, Zimbabwe*

[b]*Department of Physical Geography and Ecosystem Science, Sölvegatan 12, S-223 62, Lund, Sweden*

[c]*School of Earth and Environment, University of Leeds, Leeds, UK*

[d]*Institute of Atmospheric Physics, Chinese Academy of Science, Beijing, China*

[f]*School of Earth, Atmospheric and Environmental Sciences, The University of Manchester, Manchester, UK*

[g]*National Center for Atmospheric Research, Boulder, Colorado, USA*

*Correspondence to: *ikudzotsa@science.uz.ac.zw*: Department of Physics, University of Zimbabwe, MP 167 Mt Pleasant, Harare, Zimbabwe

Various improvements were made to a state-of-the-art aerosol-cloud model and comparison of the model results with observations from field campaigns was performed. The strength of this aerosol-cloud model is in its ability to explicitly resolve all the known modes of heterogeneous cloud droplet activation and ice crystal nucleation. The model links cloud particle activation with the aerosol loading and chemistry of seven different aerosol species. These improvements to the model resulted in more accurate prediction especially of droplet and ice crystal number concentrations in the upper troposphere and enabled the model to directly sift the aerosol indirect effects based on the chemistry and concentration of the aerosols. In addition, continental and maritime cases were simulated for the purpose of validating the aerosol-cloud model and for investigating the critical microphysical and dynamical mechanisms of aerosol indirect effects (AIE) from anthropogenic solute and solid aerosols, focusing mainly on glaciated clouds. The simulations showed that increased solute aerosols reduced cloud particle sizes by about 5 μm and inhibited warm rain processes. Cloud fractions and their optical thicknesses were increased quite substantially in both cases. Although liquid mixing ratios were boosted, there was however a substantial reduction of ice mixing ratios in the upper troposphere owing to the increase in snow production aloft. These results are detailed in the following parts of this work.

 Prepared using qjrms4.cls

Key Words: Aerosol-cloud interactions; Cloud microphysics; Cloud-resolving models; Aerosols; Aerosol Indirect

1. Introduction

According to the Intergovernmental Panel on Climate Change (IPCC) reports (Solomon et al. 2007; Boucher and Randall 2013), aerosols are one of the major climate forcing agents, they do so in two major pathways. Firstly, by directly interacting with solar radiation (Charlson et al. 1992; Liao and Seinfeld 1998; Myhre et al. 2009) and indirectly by altering the optical or radiative properties of clouds (Charlson et al. 1992; Haywood and Boucher 2000; Lohmann and Feichter 2005; O'Donnell et al. 2011; Gettelman et al. 2012). The latter pathway is referred to as the *aerosol indirect effect* (AIE) and is the subject of this paper. There is also the *semi-direct* effect, which is caused by absorbing aerosols (Lohmann and Feichter 2001; Johnson et al. 2004). These absorbing aerosols have a heating effect in the atmosphere, which may subsequently cause the evaporation of cloud particles (Johnson 2003; Hill and Dobbie 2008; Koch and Genio 2010).

Inorder to investigate the effects of the aerosols on a global scale, the use of General Circulation Models (GCMs) is required (Lohmann et al. 2007). However, these AIEs are affected by sub-grid scale microphysical processes, which are too small to resolve in coarse resolution GCMs (McComiskey and Feingold 2012). Therefore, to circumvent this challenge, aerosol-cloud microphysical processes have to be incorporated into GCMs by way of parameterizations (Menon et al. 2002a; Lohmann and Feichter 2005; Gettelman et al. 2012). These parameterizations, are developed from the use of higher resolution models, such as the Cloud System Resolving Models (CSRMs) (Phillips et al. 2009; Morrison and Grabowski 2011).

In-order to rigorously investigate and evaluate the most critical effects of aerosols on radiation via the clouds by numerical techniques, it is essential that the numerical model being used is able to resolve the relevant microphysical and dynamical cloud processes at the temporal and spatial scales that are pertinent to real clouds. Hence, the version of the numerical model used in this study is an aerosol-cloud model coupled to the Weather Research and Forecasting (WRF) model. The previous version of this model is described in Phillips et al. (2007, 2009). It was a bulk-microphysics model, which included double-moment microphysics in cloud and a single-moment in precipitation processes. The empirical parameterization for heterogeneous ice nucleation of Phillips et al. (2009) was already incorporated in that version of the model. In addition, the 2009 version of the model consisted of a semi-prognostic aerosol component responsible for the replenishment of environmental aerosols. This earlier version of the model was used to investigate the influence of increased aerosol on the microphysical properties of clouds. It was discovered that increased concentrations of primary biological aerosol particles (PBAP) boosted the number concentrations of ice crystals by about 100 % (mostly due to the intensification of both heterogeneous ice nucleation and homogeneous freezing of supercooled cloud droplets) and also at least doubled the cloud droplet concentrations mostly due to the CCN activity of extra insoluble organic particles. Also, the mean sizes of these particles were found to diminish as a result of increased competition for available vapour from extra cloud and ice particles. However, this previous version has since been transformed into a hybrid bin/bulk microphysics scheme, enabling the model to resolve essential aerosol-cloud interaction processes explicitly, while other ancillary processes were treated implicitly in-order to reduce the model's computational expense.

Double-moment schemes have proved to be superior over single moment schemes in terms of accuracy, especially in simulating precipitation in deep convective cells (Lim and Hong 2010). Due to the prediction of extra terms in double-moment schemes, their computational expense is amplified, hence, curtailing their use in real time weather forecasting and climate prediction models; however, they provide a more accurate understanding especially of cloud and precipitation processes. This is the scope within which the double-moment bulk microphysics scheme presented here was developed.

The following modifications were applied to the aerosol-cloud model, importantly to improve its performance particularly on the treatment of cloud processes that are crucial in addressing aerosol-cloud interactions. The sulphate aerosol group was dualised by splitting the two modes of sulphate aerosols (the fine and the accumulation modes) and treating them as two independent aerosol species. This development was meant to improve the

†

treatment and budgeting of aerosols especially in the activation of cloud droplets and nucleation of ice crystals. In addition to this dualisation of the sulphate aerosol species, a two-moment treatment was also incorporated for the same aerosol group. This enables a more accurate prediction of their mean sizes (which are important in the nucleation process cloud droplets and cloud ice) rather than prescribing them apriori. This special treatment was coded only for sulphate aerosols because of their dominance in the atmosphere in terms of number concentrations and their superior influence as CCN over other aerosol species.

Emulated bin-microphysics, or the explicit integration of microphysics processes has also been implemented to all coagulation processes (e.g., riming, aggregation and accretion). This explicit microphysics of coagulation processes provides a more accurate approach for treating the interaction of cloud and precipitation particles with each other. This development ensures that cloud development, changes of cloud phases and precipitation production are rigorously resolved. This was not only a major improvement to the model, but also very relevant and necessary in the research of aerosol-cloud interactions. Following the introduction of the emulated bin-microphysics approach to the coagulation processes, there was need to incorporate ice morphology into the model in order to allow accurate treatment of the collision and sticking efficiencies during particle interactions, taking into account their dependence on temperature and sizes.

A number of researchers e.g. Clark (1974); Walko et al. (1995); Mitchell and Arnott (1994) have shown that a gamma distribution is a more appropriate representation of the size distribution of hydro-meteors. Hence, in this version of the model, a gamma distribution has been used for all precipitation hydro-meteors replacing the old exponential one (Kessler 1969), which was implemented in the previous versions of the model. A common approach of fixing the intercept parameters for the size distribution was avoided here by introducing either temperature or mixing ratio dependent intercept parameters of Reisner et al. (1998); Thompson et al. (2004). This was done because a study by Reisner et al. (1998) showed that fixing the intercept parameters promoted excessive depletion of cloud water.

Since the introduction of an empirical parameterization of heterogeneous ice nucleation by Phillips et al. (2008), there has been advancement in the knowledge of the chemistry, composition and nucleating abilities of aerosols. Hence, Phillips et al. (2013) took the new available knowledge of ice nuclei and their nucleation abilities into consideration and modified his empirical parameterization. This modified version of the empirical parameterization of heterogeneous nucleation of cloud ice by Phillips et al. (2013) was also incorporated into this version of the model. The most interesting and relevant improvement here is that soluble organics are now allowed to nucleate ice-crystals at appropriate temperatures and supersaturations in line with recent laboratory observations of Murray et al. (2010).

The structure of this article is as follows. In Section 2, the aerosol-cloud model used in this study is described. The description of the cases simulated, setup and validation of the model will be given in Section 3. The discussion of the model performance and results are given in Section 4. Finally, conclusions and future work will be stated in the last Section, which is Section 5.

2. Model Description

2.1. Overview

The numerical model used here is an aerosol-cloud model coupled to the Weather Research and Forecasting (WRF) model. The original version of this model was described in Phillips et al. (2007, 2008, 2009); however, it has now been transformed into a hybrid bin/bulk microphysics scheme. Improvements to the heterogeneous ice nucleation scheme described in Phillips et al. (2013) have since been incorporated into this present microphysics scheme. This is a CSRM, which has prognostic variables of a two-moment hybrid bin/bulk microphysics for all cloud liquid and precipitation species. The CSRM is a non-hydrostatic and an an-elastic fluid flow model with periodic boundary conditions and forty vertical levels. In this study, the vertical resolution is approximately 500m, with the model-top set at 20km. The model grids are 2km wide, with the whole domain size being 170km. The integration time step of 10 seconds is being used. Prognostic microphysical variables are written out every five minutes for analysis.

For the cases simulated in this project, a two-dimensional domain is applied. Convection is maintained in a standard way

by including additional tendencies of heat and moisture. The tendencies are specified from the derived large scale forcing, observed from a network of soundings used in the respective cases simulated (see section 3.1). These tendencies are added as extra sources to the evolution equations for potential temperature and vapor mixing ratio.

2.2. *The Microphysics Scheme*

2.2.1. *The Aerosol Treatment*

The aerosol-cloud model has a semi-prognostic aerosol component (Phillips et al. 2009) comprising a complement of seven different aerosol species. The insoluble organic aerosol group is split into primary biological aerosols (PBAPs), which may include pollen, bacteria, fungal spores, viruses, plant and animal fragments and non-biological insoluble organics following (Phillips et al. 2013). In addition, the larger and smaller modes of the sulphate aerosol group are prognosed independently and treated as two different aerosol species. Furthermore, a fraction of soluble organic aerosols now acts as IN at relevant temperatures (below $-65^{\circ}C$) and supersaturations according to Murray et al. (2010). This gives an aerosol complement of nine species, each with independent prognostic variables such as mass and number mixing ratios.

These aerosols are classified into two main categories, namely, soluble and solid aerosols. The classification of the chemical composition of the aerosols follows that commonly found in some of the most modern GCM.

- The soluble aerosol species are ammonium sulphate (its bimodal distribution is separated into two independent modes as $SO4_1$ and $SO4_2$), sea-salt (SS) and soluble organic carbonaceous material (SO).
- The insoluble aerosol group comprises mineral dust/metallic (DM), soot/black carbon (BC), insoluble non-biological organic (O), primary biological aerosol particles (BIO) and finally, there is a fraction of the soluble organic group (SO) that becomes glassy at very cold temperatures (SOLO).

All species can nucleate liquid droplets; however, in the previous version of the hybrid bulk/bin microphysics scheme, solute aerosols could not nucleate ice, but, an exception has now been applied to soluble organics in line with recent laboratory observations of Murray et al. (2010). In this version, the non-biological insoluble organics do not nucleate ice heterogeneously, because they are assumed to be highly hydrophobic.

In this model, external mixing is assumed for all solute aerosol species. Insoluble aerosols (dust, soot, insoluble organics) are assumed to be externally mixed with each other, but also internally mixed with some components of soluble aerosols and therefore able to initiate cloud droplets. The soluble fractions of the respective IN groups are shown in Table 1, following Clarke et al. (2004). A log-normal distribution described by Pruppacher and Klett (1997) is assumed for all aerosol size distributions with distribution parameters of each mode (geometric mean size, spectral width, ratio of total numbers between multiple modes) being constrained by observations and in cases where observations were not available, model results from the global model for aerosol processes (GLOMAP) (Spracklen et al. 2005; Mann et al. 2010) where used instead. These parameters are shown in Table 1 for the cases simulated in this study (TWPICE and CLASIC). In this model, insoluble aerosol particles are assumed to be aged and coated with soluble components such as sulphate on their surfaces; hence enabling them to activate both cloud droplets and cloud ice.

The semi-prognostic aerosol component treats all processes that alter aerosol loadings inside clouds (wet processes). The scheme is semi-prognostic in the sense that aerosol profiles are artificially replenished by resetting them to their initial profiles at regular time intervals of three hours in both cases that were simulated in this study. This resetting of aerosol profiles is our numerically crude way to apply a large-scale advective forcing tendency for aerosol to compensate for aerosol loses in the domain. Depletion of aerosols occurs by in-cloud nucleation and precipitation scavenging. The aerosol mass and number mixing ratios are predicted; hence, the model is double moment in this regard. The model tracks the mass and number mixing ratios of aerosols in the environment (i.e. those which are not activated), in clouds and in precipitation. This makes it possible for the model to account for all the sources and sinks of every aerosol particle (AP). It is not within the scope of this study to explicitly represent changes in aerosol loading due to lateral advection of aerosols into

Aerosol group	Number of Modes	$\log_{10}$ of Standard deviation $\log_{10}(\sigma_x)$	Geometric mean, Rm_x (μm)	Solubility parameter
Sulphate (SO4)	2	0.30, 0.27; 0.049, 0.161	0.04, 0.08; 0.03, 0.18	
Sea-Salt (SS)	2;3	0.30, 0.33; 0.05, 0.16, 0.26	0.01, 0.50; 0.03, 0.18, 4.4	
Soluble Organics (SO)	2	0.30, 0.27; 0.049, 0.161	0.04, 0.08; 0.03, 0.18	
Dust/Metallic (DM)	2	0.28, 0.20	0.8, 3.0	0.15
Black Carbon (BC)	1	0.20	0.2	0.80
Insoluble Organics (O)	1	0.20	0.2	0.80
Biological Aerosols (BIO)	2	0.40, 0.60	0.17, 0.47	0.80

Table 1. *Aerosol properties; the comma separates the modes, where different aerosol specifications were applied for mid-latitude continental and tropical maritime cases, a semicolon is used with the former representing CLASIC and the latter representing TWPICE.*

and out of the domain; hence, the population of interstitial aerosols in the air is nudged towards observed/initial profiles.

2.2.2. *Size Distributions*

A Γ-distribution is applied to both precipitating (graupel (g), rain (r) and snow (s)) and size distributions for non-precipitating particles (cloud ice and cloud water) is according to Ferrier (1994). We use a shape parameter μ_r of 0 for rain, as in Ferrier (1994), whereas a value of $\mu_g = 2$ is used for graupel following Thompson et al. (2004). As for snow, a variable value of μ_s that is dependent on the mass mixing ratio (q) is based on aircraft observations of Thompson et al. (2004). These predicted values of μ_s range from -2 to 3 as prescribed by Thompson et al. (2004). For the intercept parameters, the approach of Thompson et al. (2004) is applied for rain and graupel, whereas that of Heymsfield et al. (2002) is used the intercept parameter of snow. The slope parameters (λ_x) for all the species are chosen such that they are functions of the mass mixing ratios and are predicted using Ferrier (1994) for rain, Thompson et al. (2004) for graupel and snow.

2.2.3. *Nucleation Processes*

Initiation of Cloud Droplets The initiation of cloud droplets are treated explicitly in the model as in Phillips et al. (2009). All seven aerosol species described in Sect. 2.2.1 can initiate cloud droplets. The activation of cloud particles takes place both at the cloud-base and in-cloud as long as the supersaturation is high enough to activate new cloud particles. At the cloud-base, droplet activation from solute aerosols depends on the updraft velocity and both aerosol loading and chemistry following the Ming et al. (2006) scheme. In-cloud droplet formation by solute aerosols is done by the κ-Kohler theory of Petters and Kreidenweis (2007) when in-cloud supersaturations are high enough.

Insoluble aerosols are assumed to be coated by soluble materials which enable them to initiate cloud droplets. This is treated using the κ-Kohler theory of Petters and Kreidenweis (2007) at both cloud-base and in-cloud.

Heterogeneous Nucleation of Cloud Ice As for ice nucleation, the empirical parameterization (EP) of heterogeneous ice nucleation developed by Phillips et al. (2008) was updated to include improvements made in the Phillips et al. (2013). The EP model still allows nucleation from all known modes of heterogeneous ice nucleation (*deposition, condensation, immersion* and *contact freezing*) and most importantly, the scarcity of ice nucleation at sub-saturated conditions and the dependence of IN on the total surface area of each aerosol species are still treated by the EP. The main property used by the EP scheme for heterogeneous ice-nucleation is the baseline total surface area of all IN, whose sizes are greater than a minimum threshold of 0.1μm. The current version of the EP has had a myriad of changes which include allowing soluble aerosols to nucleate ice crystals at very cold temperatures as detailed Phillips et al. (2013).

Homogeneous Freezing of Cloud Droplets and Aerosols Homogeneous freezing of cloud droplets takes place at -36°C. Preferential freezing is assumed, i.e., larger droplets freeze first depending on supersaturation and ascent velocity according to the parameterization of Phillips et al. (2007). Consequently, nucleation and rapid condensational growth of ice crystals ensues that leads to a reduction of supersaturation. If the water vapour dips below saturation then the smaller cloud droplets start evaporating which can mantain the cloud close to water saturation, thus, total evaporation may occur for some of the small cloud

droplets without freezing. The parameterization also monitors the fraction of cloud droplets that do not freeze. Also, homogeneous freezing of interstitial aerosols is applied at cold temperatures at high relative humidities near water saturation, taking into account the curvature and surface tension effects at temperatures below -40°C.

Ice Multiplication Secondary multiplication of cloud ice by the Hallet-Mossop process is modified from that of Phillips et al. (2009) and treated in the model at temperatures, T between -3°C and -8°C by assuming that for every milligram of liquid being accreted onto snow or graupel per unit time, a total of 350 small ice crystals with initial diameters of 5μm are ejected at -5.5°C as:

$$NIHMS = 350.e^{6} f_{HM} T_{HM} PSACW \tag{1}$$

$$NIHMG = 350.e^{6} f_{HM} T_{HM} PGACW \tag{2}$$

where, f_{HM} is a increasing droplet-size dependent factor, which requires that no splinters be ejected by droplets of sizes less than 16μm and can be represented as:

$$f_{HM} = \begin{cases} 0., & \text{if } D_{CW} < 16\mu m, \\ 1., & \text{if } D_{CW} > 24\mu m, \\ \frac{D_{CW}-D_{min}}{D_{max}-D_{min}}, & elsewhere \end{cases}$$

where, D_{CW} is the cloud droplet diameter, while D_{min} and D_{max} are the minimum and maximum thresholds of droplet sizes for the parameterization, which are respectively 16 and 24 μm. The factor T_{HM} is a triangular function of temperature which ensures that the maximum number of H-M splinters are ejected at $-5.5°C$ per hydrometeor.

$$T_{HM} = \begin{cases} \frac{8-|T|}{2.5}, & \text{if } -5.5 >= T > -8, \\ 0., & \text{if } T <= -8..or.T > -3., \\ \frac{|T|-3}{2.5}, & \text{if } -3 >= T > -5.5 \end{cases}$$

2.2.4. *Autoconversion Processes*

All the auto-conversion processes, e.g. of cloud-droplets to rain, cloud-ice to snow and snow to graupel are being treated using a bulk parameterisation approach detailed below.

The Autoconversion of Cloud Droplets to Rain The rate of autoconversion of rain from cloud particles, PRAUT, is treated using the scheme of Khairoutdinov and Kogan (2000) (Eqn. 3).

$$PRAUT = 1350 q_c^{2.47} n_c^{-1.79} \tag{3}$$

This is a robust bulk parameterization based on the results of a bin-resolving model. It depends primarily on predicted cloud droplet number and mass mixing ratios n_c and q_c, respectively.

The Autoconversion of Cloud Ice to Snow The rate of conversion of cloud ice to snow follows a modified version of Ferrier (1994)'s parameterization when the slope parameter, λ_i, of the ice crystal size distribution exceeds a certain minimum threshold, λ_{i0} (Eqn. 4).

$$PSAUT = \frac{q_i}{\Delta t}\left(1 - \left(\frac{\lambda_i}{\lambda_{i0}}\right)^3\right) \tag{4}$$

where, $\lambda_{i0} = \Gamma(2+\mu_i)/(150e^{-6}\Gamma(1+\mu_i))$ for the shape parameter, μ_i and Δt is the model time-step.

The Autoconversion of Snow to Graupel The autoconversion of snow to graupel (PGAUT) is dependent on the riming rate of cloud liquid onto snow. It is determined by deducting the sum of mass mixing ratios of snow gained by depositional growth (PSDEP) and accretion of cloud ice (PSACI) from the total mass gained by snow through riming (PSACW). Half of this difference becomes the mass of graupel gained through autoconversion (Eqn. 5). This treatment follows the semi-empirical treatment developed by Swann (1998) and requires the snow content to exceed a critical threshold of 500μg.

$$PGAUT = 0.5(PSACW - PSDEP - PSACI) \tag{5}$$

Here, PSDEP is determined following the bulk parameterization of Lin et al. (1983). For the rates of changes of the number mixing ratios from the autoconversion processes, NRAUT, NSAUT and NGAUT, a critical radii of the new seeds of these species are prescribed, which are $50\mu m$ for rain $170\mu m$ for snow and finally $100\mu m$ for graupel.

2.2.5. Coagulation Processes

An emulated bin microphysics approach has been incorporated into the model for the coagulation processes shown in Table 3 below.

A mass grid $m_x(D_x)(j)$ of 33 sizebins is populated using Eqn. 6 by prescribing a minimum diameter $D_{min,x}(j)$ at $j = 1$ for each $x = g, i, s, r, l$ and incrementing the mass from one size-bin to the next using an arbitrary multiplication factor.

$$m_x(D)(1) = \frac{\pi \rho_x D_{min,x}^3}{6} \tag{6}$$

Where ρ_x is the bulk density of the xth species.

The change in mass mixing ratio per unit time, $\frac{\Delta q_{x,y}}{\Delta t}$ of specie x, collecting specie y can be computed as:

$$\frac{\Delta q_{x,y}}{\Delta t} = \sum_{i=1}^{N_t} \sum_{j=1}^{N_t} \chi_{x,y}(i,j) n_x(i) n_y(j) m_y(j) \tag{7}$$

and like-wise, the change in number mixing ratio per unit time, $\frac{\Delta n_{x,y}}{\Delta t}$

$$\frac{\Delta n_{x,y}}{\Delta t} = \sum_{i=1}^{N_t} \sum_{j=1}^{N_t} \chi_{x,y}(i,j) n_x(i) n_y(j) \tag{8}$$

where, i and j are indices of summation through the N_t mass-grids, $\chi_{x,y}$ is the collection kernel for the interacting particles x and y, N_x and M_x are respectively, the number and mass mixing ratios of the interacting species. These changes in mixing ratios per unit time equal the mixing ratio tendencies that are added to the evolution equations of mass and number mixing ratios at every model time step.

Collection Kernels The collection kernel, $\chi_{x,y}$, for the interacting particles x and y is propotional to the volume swept by the particles per unit time falling at relative fall velocity, $V_t = |V_{t,x,sfc}(i) - V_{t,y,sfc}(j)|$ and is given by:

$$\chi_{x,y}(i,j) = E_{c,x,y}(i,j) E_{s,x,y} A_{x,y}(i,j) V_t \sqrt{\frac{\rho_{sfc}}{\rho_a}} \tag{9}$$

where, $E_{c,x,y}$, is the collision efficiency of collisions between particles x and y, values of which are interpolated from the Explicit Microphysics Model (EMM) results of Phillips et al. (2005). $E_{s,x,y}$ is the sticking efficiency between collisions of particles x and y. The geometric cross sectional area, A_{xy}, is given by:

$$A_{x,y}(i,j) = \pi (D_x(j)/2 - D_y(j)/2)^2 \tag{10}$$

$V_{t,x,sfc}$ is the terminal velocity of the hydrometeor of diameter, $D_{x,y}$, evaluated at the surface using an expression of the form of Eqn. 11, where the coefficients are as given in Heymsfield et al. (2007a).

$$V_t(D) = aD^b \tag{11}$$

The last term on the right in Eqn. 9, with surface air density, ρ_{sfc}, and air density, ρ_a, at a given model level is the altitude correction factor for the terminal velocity.

Sticking Efficiencies The sticking efficiencies, $E_{s,x,y}$ (Eqn. 12) for the collisions between the solid particles are computed using a new empirical parameterisation developed by Phillips et al. (2015) using a long history of laboratory observations available in the literature. In Phillips et al. (2015), $E_{s,x,y}$ is given by:

$$E_{s,x,y} = \exp^{\frac{\beta(T) K_c}{\alpha}} \tag{12}$$

where, $\beta(T)$ is a temperature-dependent thermal smoothness coefficient that caters for the surface texture of the particles. K_c is the collision kinetic energy of the colliding particles and is proportional to the energy required to separate the particles after impact, while α is the surface area of the smaller particle involved in the collisions. Wet-growth of graupel is also being treated in this aerosol-cloud model, hence in the case of wet-growth of graupel, a sticking efficiency of unit is assumed for collisions between graupel and other solid hydrometers following Musil (1970). For collisions involving cloud liquid and rain, a sticking efficiency of unity is also imposed.

Turbulence Enhancement Enhancement of accretion by turbulence is also treated in this hybrid bin/bulk aerosol-cloud model. This is done by a simplified version of the turbulence enhancement scheme developed for the Hebrew University cloud model by Benmoshe and Khain (2014). The difference between our approach and that of Benmoshe and Khain (2014) is that we do not explicitly calculate the turbulent kinetic energy, which

is used to determine the dissipation rate, but we empirically parameterize the dissipation rate using the data of MacPherson and Isaac (1977). The parameterization of dissipation rate, ϵ that we use is a function of vertical velocity, w and is given by:

$$\epsilon = 0.00954|w| \tag{13}$$

This is the turbulence enhancement factor that is applied to all collisions in mixed-phase clouds.

2.2.6. *Melting*

Melting of ice is based on Eqns. 16-80 of Pruppacher and Klett (2010) and in this approach, processes for all solid hydrometeors are treated explicitly in the model. The tendencies of mass and number mixing ratios, PXMLT and NXMLT (for X = G or S or I) from the melting process are treated as sources of both number and mass mixing ratios for rain.

2.2.7. *Sedimentation of Hydrometeors*

A bulk microphysics approach is still being used for evaluating the fall velocities of the hydrometeors following the approach of Ferrier (1994). A number weighted fall velocity is used for the sedimentation of the number mixing ratios and a mass weighted fall velocity is used for the fall velocity of the mass mixing ratios.

3. Model Comparisons to Observations

To ensure the model is in agreement with observations, we compare results from our model simulations to two cases of observations. We compare to ARM data from aircraft, satellite and ground-based observing platforms for the continental case (CLASIC) and the maritime case (TWPICE). The comparisons to observations were done in close collaboration with the aircraft scientists who were involved in the respective campaigns so as to interpret the observational data properly. Detailed descriptions of these campaigns are given in (May et al. 2008; Fridlind et al. 2009; Allen et al. 2008; Kudzotsa 2013).

3.1. *The Simulated Cases*

3.1.1. *The Tropical Warm Pool International Cloud Experiment (TWPICE)*

The Tropical Warm Pool International Cloud Experiment (TWPICE) (May et al. 2008) was a three-and-a-half weeks long maritime case of deep convection. It was carried out from the 17^{th} of January to the 12^{th} of February in 2006 over Darwin, in north western of Australia (lat = -12.425° and lon = 130.891°). The campaign comprised of both a dense network of ground-based, including ship, and air-borne observations. A fleet of four aircraft participated in the campaign flying at low and high altitude, sampling the whole column of the atmosphere up to the lower stratosphere. The campaign covered a region with a radius of about 150 km. This case is ideal for assessing our aerosol-cloud model because of the availability of spatially extensive and temporally continuous microphysical and thermodynamic data.

The flight patterns for the high altitudes flights were aimed at sampling the microphysical and aerosol properties of the cirrus clouds; hence, the flight patterns were designed to sample both the fresh anvil outflow and also the aged cirrus. As for the low level flights, the flight patterns were designed to sample the boundary structure.

Meteorological Conditions During the active monsoon period, there was a persistence of cirrus overcast conditions over the whole domain and a prevalence of organized deep convection with cloud-tops reaching as high as the tropopause, hence the fresh anvil outflow with aged cirrus (May et al. 2008). The airflow during this period was westerly from the surface up to 300mb (Allen et al. 2008). This weather pattern persisted from the 17th to the 22nd of January. From the 23rd, the monsoon was suppressed and this persisted until the 2nd of February and, was characterized by a deep inland low that drove stable westerly airflow into the domain. Although a quasi-static mesoscale convective system (MCS) developed during this period, convection was suppressed and the cloud-tops during this period rarely exceeded the 10km altitude (May et al. 2008; Allen et al. 2008). From the 3rd of February, an easterly airflow at 700mb developed and was followed by three days of clear skies. In the days following the

clear skies, scattered convection prevailed, which developed into a more organized multi-cellular system during the later stages of the monsoon break period (May et al. 2008).

3.1.2. *The Cloud and Land Surface Interaction Campaign (CLASIC)*

The Cloud and LAnd-Surface Interaction Campaign (CLASIC) (Miller 2007) was a three-weeks long continental campaign studying deep convection. It was carried out from the 10^{th} to the 30^{th} of June in 2007 over the research facility of the U.S Department of Energy (DOE) called the Atmospheric Radiation Measurement-Climate Research Facility - Southern Great Plains (ARM-SGP) Oklahoma, U.S (lat = 36.61° and lon = 97.49°).

Meteorological Conditions The campaign period for CLASIC was characterized by the wettest summer on record for the city of Oklahoma. It was caused by the existence of a quasi-permanent high-pressure cell that established over the south eastern USA for much of the campaign period. This high-pressure system drove low-level southeasterly airflow into Oklahoma, advecting moisture from the Gulf of Mexico. At the upper levels, a couple of slow moving upper level troughs, coupled with this low-level pattern caused persistent convective conditions accompanied by significant amounts of rainfall during the campaign. The conditions resulted in frequent shallow convection to be the dominant process leading to clouds during the CLASIC campaign period.

3.2. *The Model Setup*

In addition to general specifications of the model given in Sect. 2.1, further conditions were applied to the model depending on the campaign being simulated. The model was initialized using domain averages of observed thermodynamic (vapour and temperature) profiles. Their corresponding thermodynamic tendencies, together with profiles of horizontal wind and pressure were used as large-scale forcing. Of this large-scale forcing, only temperature was nudged at each time step, towards observed values with a relaxation time scale of three hours. This nudging was only done above the 15 km altitude. Convection was initiated using random perturbations of moisture in the lower troposphere. It was maintained by including additional tendencies of heat and moisture due to the observed large-scale advection from a network of soundings in the simulated cases.

Aerosol profiles were prescribed for the whole model domain using aircraft observations for the simulated cases. In the instances of lack of observations, data from other similar campaigns in similar regions that were conducted concurrently with the campaign were used. Further details for each campaign are outlined below.

3.2.1. *The Tropical Maritime Case - TWPICE*

A quasi-maritime and quasi-land initialization was applied to model the TWPICE case, since the campaign domain was approximately 50% over land and 50% over the ocean. A fixed sea-surface temperature of 29°C was applied following Fridlind et al. (2009); Fridlind and Co-authers (2012); Morrison and Grabowski (2011).

The aerosol data in Fig. 1 was derived from Allen et al. (2008). This aerosol data was obtained during the ACTIVE campaign, a sister campaign of TWPICE. For the TWPICE case, there was no aerosol data obtained during the campaign and so we used aerosol data from the ACTIVE campaign in its place. ACTIVE was a sister campaign studying similar convective conditions in Darwin. The campaign was conducted between November of 2005 and February of 2006 over Darwin, Australia (lat = -12.425° and lon = 130.891°). There was one aircraft deployed during the campaign, the Dornier 228-101 aircraft. Dornier profiled the

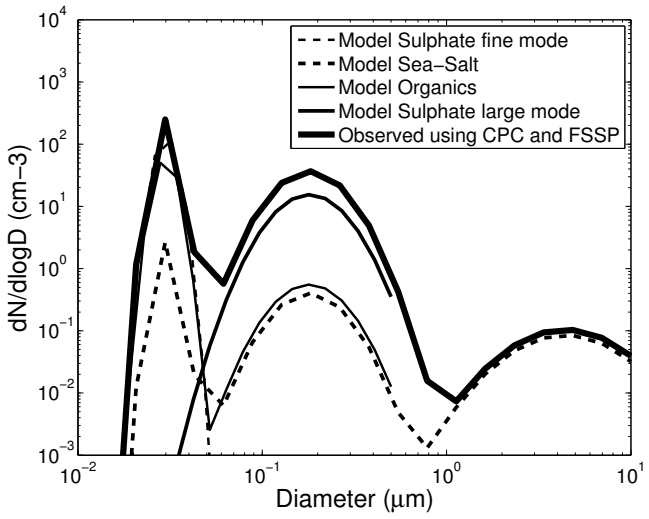

Figure 1. *A tri-modal aerosol size distribution applied to the model for TWPICE case. Distribution parameters given by Fridlind et al. (2009), taken from Allen et al. (2008) have been applied. The species are explained in the legend.*

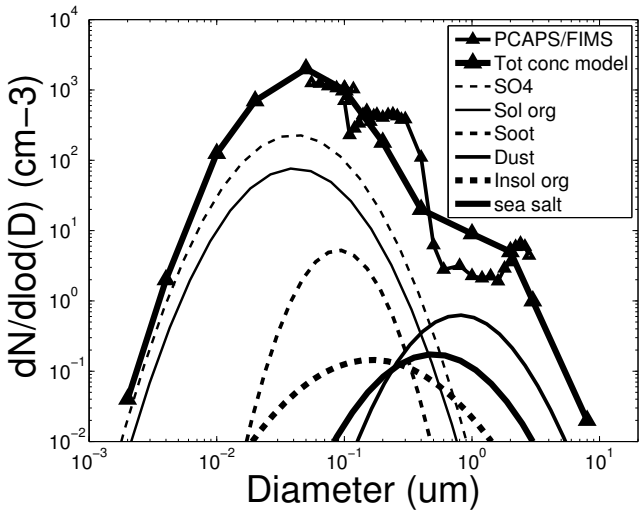

Figure 2. *A tri-modal aerosol log-normal size distribution applied to the model for CLASIC case. Distribution parameters prescribed by Phillips et al. (2009) have been applied. The respective species are as explained in the legend.*

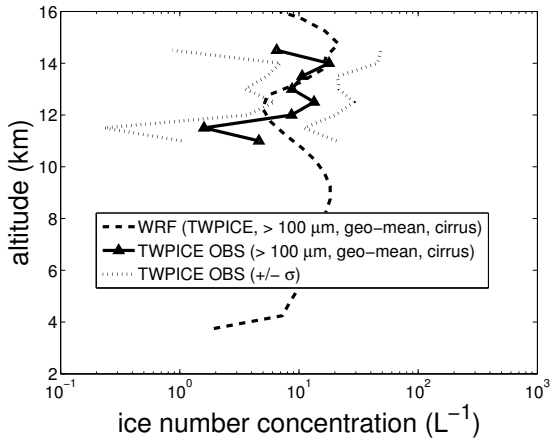

Figure 3. *Mean number concentrations of crystals with effective diameters greater than 100 µm for TWPICE. The solid lines represent the average values, while the broken lines represent standard deviations from the mean. The blue lines represent the model results, while the red ones are for observations. Conditionally averaged over regions of weak vertical velocities (vertical velocity less than 1. m s^{-1}) and cloudy regions with IWC greater than 0.001 gm^{-3}.*

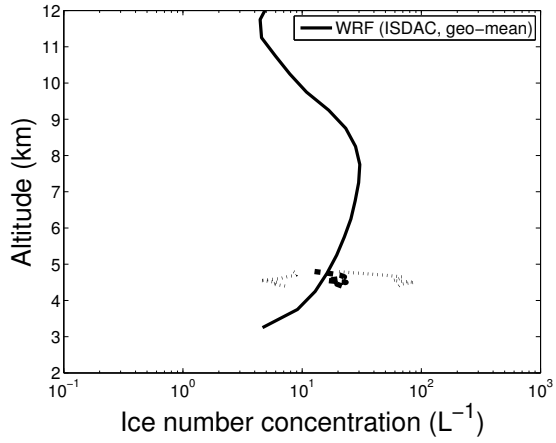

Figure 4. *Mean number concentrations of crystals with effective diameters greater than 100 µm for CLASIC. The solid lines represent the average values, while the broken lines represent standard deviations from the mean. The blue lines represent the model results, while the red ones are for observations. Conditionally averaged over regions of weak vertical velocities (vertical velocity less than 1. m s^{-1}) and cloudy regions with IWC greater than 0.001 gm^{-3}.*

lower troposphere for aerosol physico-chemical properties and measured sulphate, sea-salt and organic aerosols. We assumed primary biological aerosol particles (PBAPs) to be 50% of the measured insoluble organics (Pruppacher and Klett 1997). Black carbon (soot) and dust were not measured during the campaign; hence, we used outputs from a global tracer model, the global model of aerosol processes (GLOMAP). At higher altitudes where in-situ measurements were not taken, the aerosols were extrapolated as homogeneously mixed and equal to the concentrations at the highest altitude taken. This is similar to how other researchers (Fridlind et al. 2009; Morrison and Grabowski 2011) have treated the problem. A lognormal distribution (Fig. 2) with distribution parameters similar to those prescribed by Fridlind et al. (2009) in their model inter-comparison study and from Matthias-Maser and Jaenicke (1995) for carbonaceous and PBAPs was adapted. The simulation was run based on the data from the 17th of January 2006 at 0300Z and ending at midnight of the 12th of February 2006.

3.2.2. *The Mid-Latitude Continental Case - CLASIC*

As for the CLASIC case, continental specifications were imposed and a Γ-distribution was also assumed for the aerosols. The aerosol data were acquired from the CHAPS campaign (Berg et al. 2009), a sister campaign of CLASIC that was conducted concurrently with CLASIC. The focus of CHAPS was to obtain detailed physical, chemical and radiative properties of CCN and aerosols in general from urban pollution and contrast with their natural fields. The distribution parameters prescribed by Phillips et al. (2009) shown in Table. 1 were used for the aerosol distribution. For aerosol profiles at altitudes above the flight ceilings, the same extrapolation technique applied for TWPICE above was also used here. The simulation was commenced at 0000Z of 10 June 2007 and ran to the midnight of 30 June 2007. For both cases, the model output was written out at 5-minute intervals of the simulation time and 36 hours of the model spin-up were allowed before the analysis of the model results.

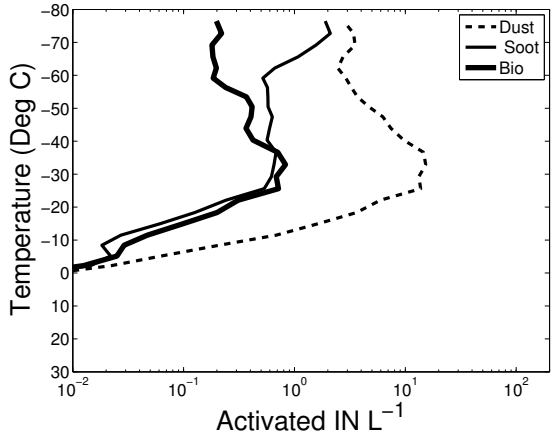

Figure 5. *The number budgets of activated IN in TWPICE*

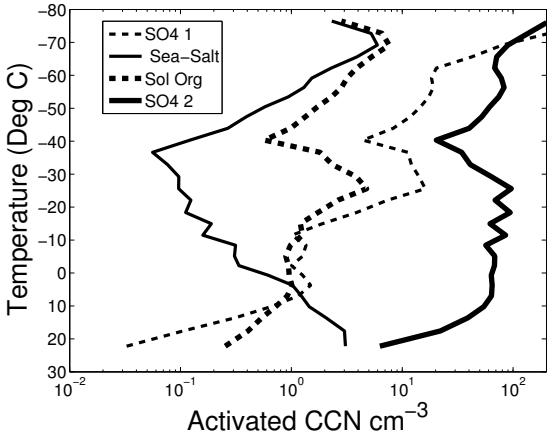

Figure 7. *The number budgets of activated CCN in TWPICE control run.*

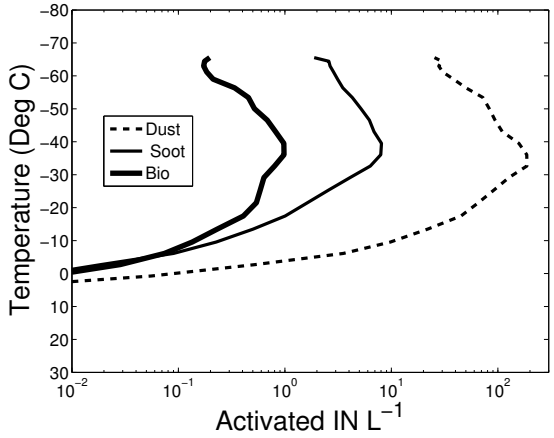

Figure 6. *The number budgets of activated IN in CLASIC*

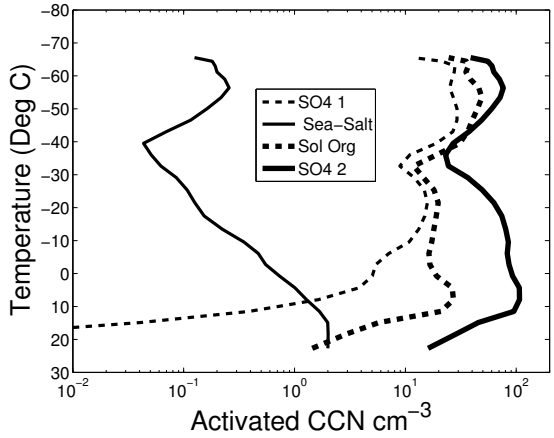

Figure 8. *The number budgets of activated CCN in CLASIC control run.*

4. Results and Discussion

4.1. Microphysical Properties

4.1.1. Ice Crystal Number Concentrations

In Fig. 3 and 4, the vertical profiles of ice number concentration for the predicted and observed values are shown. For TWPICE, the model prediction lied within the 90% confidence interval of the population mean. This was the case for the regions where comparison with observations was possible due to the availability of observations. The red curve in the figure 3 represents the observations and it represents an average of flight measurements from nine days taken during the campaign using the Cloud Imaging Probe (CIP).

The CIP probe (as explained above) counted all particles with diameters between 25 and 2300 μm. This size range includes giant aerosols, cloud droplets and cloud ice. We note that at altitudes above the 10km fight level, negligible amounts of giant aerosols (diameters $>$ 25 μm) exist, owing to gravitational effects and due to the onset of homogeneous freezing of cloud droplets at around the 9km altitude in TWPICE, no cloud droplets would be expected in this CIP data. There is an issue of ice shattering that tends to inflate crystal number concentrations and could be acting in these observations so to address this, the CIP data was corrected for ice shattering by imposing cut-off sizes of 100μm in the observed data. Hence, both the predicted and observed concentrations in Fig. 3 are for ice crystals of sizes greater than 100μm.

The aerosol types nucleating ice are shown as height profiles in Figs. 5 and 6. They show that dust is the dominant source of heterogeneously nucleated ice crystals in the model for both TWPICE and CLASIC; however, soot and biological aerosols still have substantial contributions to the total number concentration of heterogeneously nucleated ice crystals. It should however be noted that homogeneous aerosol and cloud droplet freezing are by far the most dominant sources of ice crystals as shown in part II of this work. The Halett-Mossop process (see section 2.2.3), which is an ice multiplication process is the second most significant source of ice crystals in the model.

Observational data for ice crystal number concentrations are limited for CLASIC (Fig. 4). This is because most of the flights during the campaign traversed only the lower troposphere, where water clouds were prevalent. However, we find the order of magnitudes of the predicted ice number concentrations are in good agreement with those found by other researchers (Mitchell 1994; Kajikawa and Heymsfield 1989) in their modeling and observational studies.

The higher ice number concentrations in CLASIC relative to TWPICE are expected for ocean and land conditions. There were higher aerosol number concentrations in the continental CLASIC than in the maritime TWPICE. The CLASIC aerosol scenario was very polluted as it was conducted near and downwind of urban areas in Oklahoma.

A peak in ice number concentration (due to homogeneous freezing of cloud droplets and aerosols) is seen in both simulations, although it is more distinct in CLASIC than in TWPICE. This is mainly because homogeneous freezing is more favorable in continental than in maritime clouds because of the smaller sizes of cloud particles that characterize continental clouds relative to maritime clouds. Smaller sizes of cloud particles delay the onset of rain; hence, clouds have a higher chance of growing deeper to reach the homogeneous freezing levels.

4.1.2. Cloud Droplet Number Concentrations

By referring to both Figs. 7 and 8 which are showing the number budgets of the sources of cloud droplets from all the different aerosol species being treated in the model, it can be seen that the accumulation mode of sulphate aerosols is the dominant source of cloud droplets, especially in TWPICE. In CLASIC however, soluble organics are equally important because of the relatively high soluble organics to sulphur ratio in CLASIC compared to TWPICE.

A Forward Scattering Spectrometer Probe (FSSP) mounted on the wing of the Dornier aircraft during the ACTIVE campaign measured droplet number concentration. The FSSP probe measures particles with sizes ranging from 0.5 - 32 μm and has the potential to include super-micron aerosols in its measurements of cloud droplet concentrations, hence, a minimum threshold for LWC of 0.001 gm^{-3} was imposed for cloud screening for FSSP data. Figures 9 and 10 show the average vertical profiles of droplet number concentrations for TWPICE and CLASIC, respectively. The observations curve in Fig. 9 is an average of flight measurements taken from fourteen days of the campaign. The model results were conditionally averaged over regions of weak vertical velocities, where the magnitudes of vertical velocities were less than 0.5m s^{-1}. This was done to match the flight patterns of the campaign; the Dornier aircraft always avoided cores of convection to avoid severe turbulence. Also, all the ACTIVE and TWPICE flights did not specifically target and sample liquid phase clouds although there were occasional passages through shallow cumulus cloud.

For CLASIC, the Cloud, Aerosol and Precipitation Spectrometer (CAPS) probe measured the droplet number concentrations.

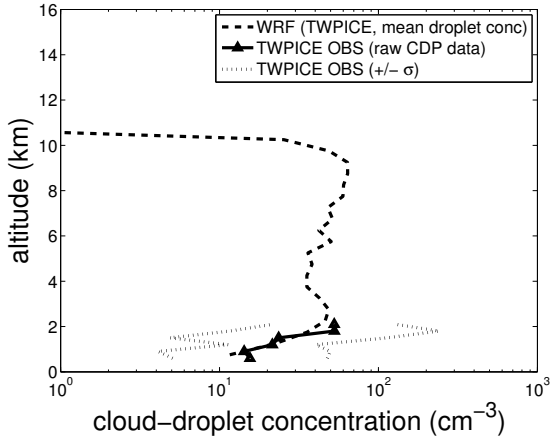

Figure 9. *Mean number concentrations of cloud droplets for the TWPICE campaign. Conditionally averaged over regions of weak vertical velocities (vertical velocity less than 0.5 m s^{-1}) and cloudy regions with ice water content greater than 0.001 gm^{-3}. The solid lines represent the average values, while the broken lines represent standard deviations from the mean. The blue lines represent the model results, while the red ones are for observations.*

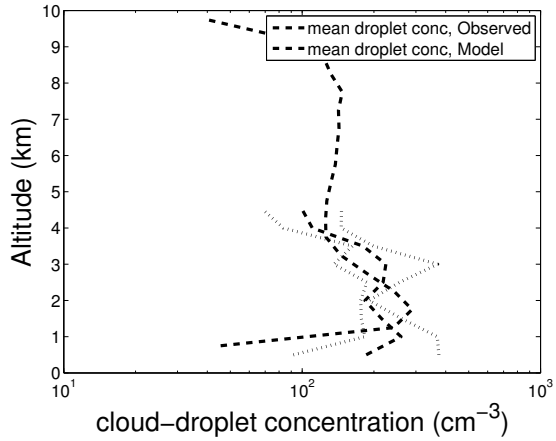

Figure 10. *Mean number concentrations of cloud droplets for the CLASIC campaign. Conditionally averaged over regions of strong vertical velocities (vertical velocity greater than 0.5 m s^{-1}) and cloudy regions with ice water content greater than 0.001 gm^{-3}. The solid lines represent the average values, while the broken lines represent standard deviations from the mean. The blue lines represent the model results, while the red ones are for observations.*

The CAPS comprises the Cloud Aerosol Probe (CAS) and the Cloud Imaging Probe (CIP) for measurements within the 0.5 to 50 and the 25 to 1550 μm size ranges. The observations shown are an average of flight measurements using the CAPS probe for size bins between 5 and 50 μm (our thresholds for cloud particle sizes) taken from thirteen different days of the campaign. Cloud screening was performed by selecting instances where the LWC was greater than 0.013gm^{-3} to eliminate instances were only aerosols were detected by the CAS at its lowest sizes of the measured spectrum. CLASIC was characterized by shallow convection producing heavy precipitation, so the comparison to observations is done by conditionally averaging the predicted number concentrations of cloud droplets over clouds with vertical velocities greater than 0.5m s^{-1}.

Satisfactory agreement between observations and model results is seen in Figures 9 and 10, showing the strength of the model in resolving these microphysical processes. Also, the higher cloud droplet number concentrations in CLASIC relative to TWPICE are explainable in terms of their contrasting aerosol scenarios (as explained for ice crystal concentrations). The strong peaks in cloud droplet concentrations shown at 2km altitude are reminiscent of the one expected at cloud bases. Since, supersaturations attain their maximum values within a few meters above cloud-base and decrease gently to a steady value beyond that level, so does the droplet number concentration (Rogers and Yau 1991). The other explanation is the onset of collision and coalescence aloft, which depletes cloud number through rain production. Finally, because of preferential sedimentation of larger cloud droplets that peak can also not be averted.

4.1.3. *Mean Radius of Ice Crystals*

The mean sizes of cloud ice are important in assessing the radiative properties of clouds, for instance in the determination of the extinction coefficient (Mitchell 1994), which is a measure of how strongly a substance attenuates the radiative fluxes. Therefore, the model predicts the mean sizes of cloud-ice and results are shown in Figs. 11. A good agreement between observations and model predictions is noted for TWPICE (Fig. 11). The decrease of mean crystal sizes with height is primarily due to an increase with height of the total number concentrations of ice particles (Figs. 3 and 4), which increases the competition for the same amount of available vapour. Sedimentation of ice crystals out of cirrus clouds and the growth of crystals by vapour diffusion promotes riming and aggregation during descent. Other mechanisms of crystal growth such as aggregation are also effective in higher temperatures. No comparison with observations is shown for CLASIC due to the unavailability of ice-phase data; however, predictions were quite realistic with reference to TWPICE (plot not shown).

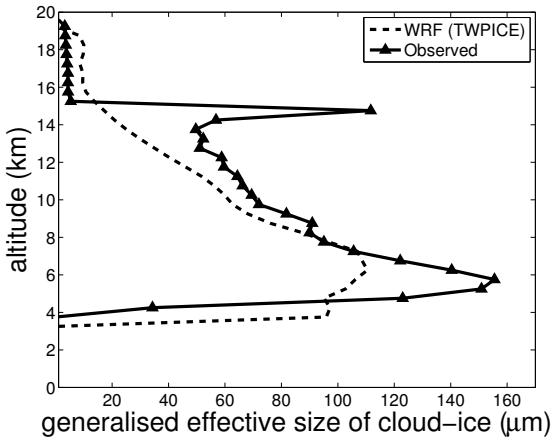

Figure 11. *Vertical profiles of mean effective diameter of ice crystals for TWPICE. Conditionally averaged over cloudy regions where effective crystal diameter was greater zero. The solid lines represent the average values, while the broken lines represent standard deviations from the mean. The blue lines represent the model results, while the red ones are for observations.*

4.2. *Macrophysical Properties and Radiation Statistics*

4.2.1. *Precipitation*

Figures 12 and 13 show area averaged cumulative precipitation that is unconditionally averaged over the whole domain of the study and over the whole simulation period for both TWPICE and CLASIC, respectively. A 'near-perfect' agreement between model predictions and observations is predicted in both simulations particularly for TWPICE.

4.2.2. *Radiation Statistics*

Table 2 shows the radiation statistics for the upward and downward components of radiation measured at the top of the atmosphere (TOA) and at the surface for both TWPICE and CLASIC. The observations statistics were downloaded from the ARM's website (`www.arm.com`), where they are available freely for both cases.

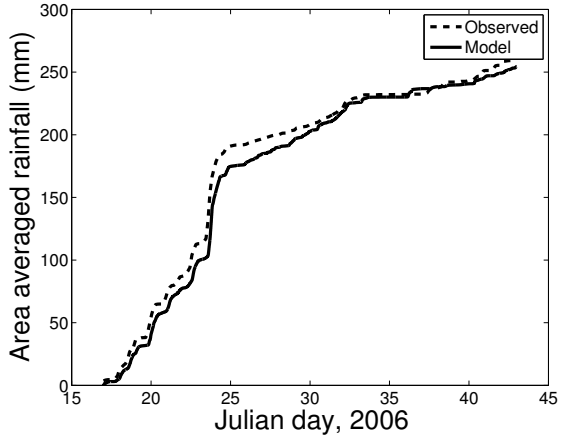

Figure 12. *Cumulative precipitation in mm unconditionally averaged for the whole four-week simulation period of TWPICE. The solid lines represent the average values, while the broken lines represent standard deviations from the mean. The blue lines represent the model results, while the red ones are for observations.*

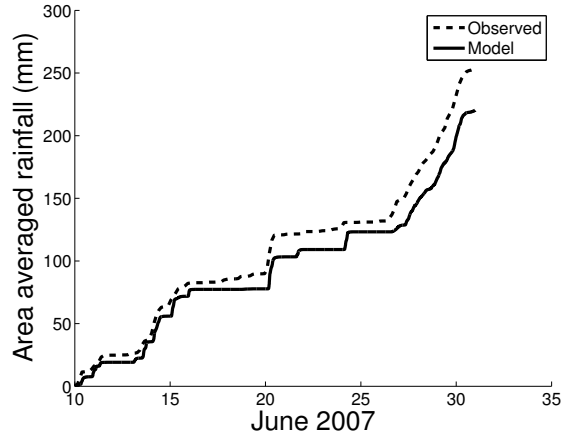

Figure 13. *Cumulative precipitation in mm unconditionally averaged for the whole three-week simulation period of CLASIC. The solid lines represent the average values, while the broken lines represent standard deviations from the mean. The blue lines represent the model results, while the red ones are for observations.*

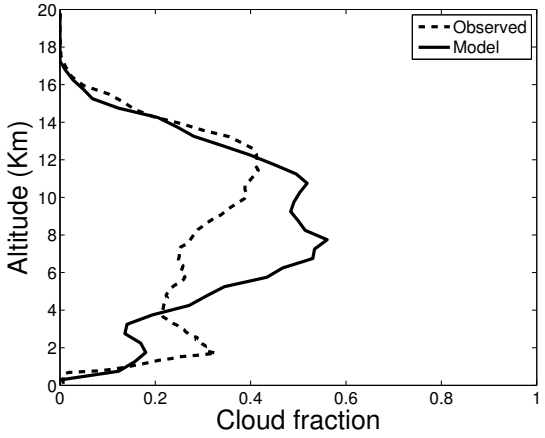

Figure 14. *Vertical profile of cloud fraction for TWPICE averaged over the whole simulation domain for cloud mixing ratios greater than 0.01 gkg^{-3}. The blue line represents the model mean, while the red line represents the observed mean.*

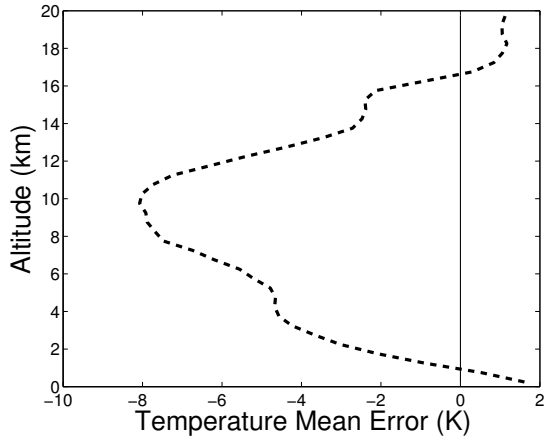

Figure 15. *Unconditionally averaged vertical profile of temperature bias (model mean minus observations mean) for TWPICE.*

The highest percentage bias of 33.75% for the upward component of SW radiation at the top of the atmosphere for TWPICE was attributed to the fact that the model predicted higher middle level cloudiness than observations (Fig. 14), this would imply a higher optical depth and, hence, higher reflectivity in the SW range by clouds. Still on the same campaign, the negative bias of -5.56% in the downward component of the long-wave radiation at the surface was also attributed to the higher reflectivity of long-wave radiation in the model by clouds, since the the model predicted more middle level clouds. This negative bias was also augmented by the strong temperature dependence of the emitted radiative flux (Stefan-Boltzmann law). Fig. 15 and 16 show that the model is generally colder than observations, implying that the predicted clouds would be colder than the observations; hence, long-wave radiation emitted downwards by the predicted clouds was lower than the observed.

For CLASIC, it is not immediately explainable from the available analysis why a higher positive bias of 17% is available for the downward component of short-wave radiation at the surface, but, parsimonious evidence available in Fig. 17 suggests that on average, the model predicted slightly less cloudiness than observations, and thus, more insolation was transmitted to the surface and also, the model systematically predicted less LWC than observations, hence, the optical thicknesses of clouds predicted in the model were less than those of observed clouds. All other biases are within an acceptable absolute deviation from observed values of less than $\pm 10\%$. This satisfactory model performance for the radiation statistics is crucial for the core objective of this study, which is the investigation of aerosol-cloud interactions. Because accurate assessment and quantification of optical properties of clouds require high confidence in prediction of radiative fluxes, both at the top of the atmosphere and at the surface.

Radiation fluxes (Wm^{-2})	SW TOA upwards	SW SFC downwards	LW TOA upwards	LW SFC downwards
Model TWPICE	174.16	213.36	210.12	404.23
Observed TWPICE	130.22	216.06	201.88	428.16
Percentage bias (%)	33.75	-1.25	4.08	-5.56
Model CLASIC	196.69	240.36	199.89	371.10
Observed CLASIC	184.26	206.32	225.04	403.82
Percentage bias (%)	6.74	16.50	-11.17	-8.10

Table 2. *Unconditionally averaged statistics for upwards and downwards components of radiation for TWPICE and CLASIC. The abbreviations are as follows: SW = Short-Wave, LW = Long-Wave, TOA = Top Of the Atmosphere, SFC = SurFaCe.*

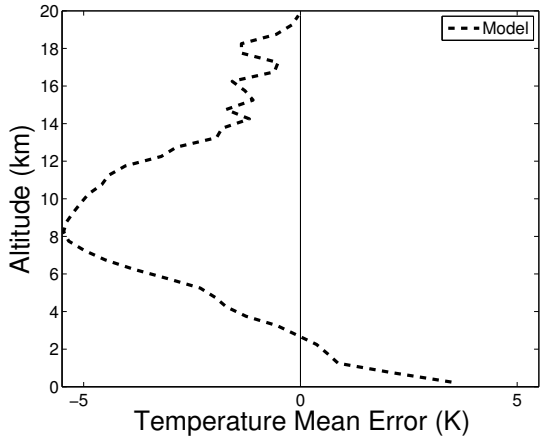

Figure 16. *Unconditionally averaged vertical profile of temperature bias (model mean minus observations mean) for CLASIC.*

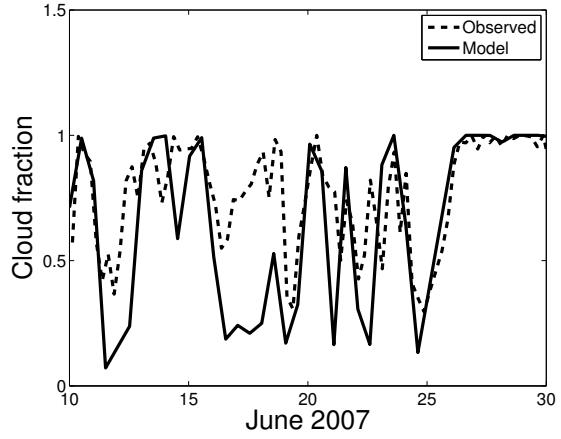

Figure 17. *Time series of cloud fraction for CLASIC averaged over the whole simulation domain for cloud mixing ratios greater than 0.01 gkg^{-3}. The blue line represents the model mean, while the red line represents the observed mean.*

5. Conclusions

A series of model developments were carried out in this study as clearly elaborated in Sect. 2. Subsequently, the comparison of the model results with observations were performed by simulating two contrasting tropical scenarios of deep convection, the Tropical Warm Pool-International Cloud experiments (TWPICE) and Cloud and LAnd Surface Interactions Campaign (CLASIC), which are respectively maritime and continental. Some of the fields compared with observations have been presented in the results sections. The comparison of the model results to observations has shown (where comparison was possible) satisfactory agreement between model simulations and observations and the model standard deviations being within a reasonable range of less than 40% of the model mean values. The available observation dataset was obtained from a dense network of ground-based observation platforms, aircraft, ships and satellites.

Predictions of both crystal and droplet number concentrations have lied within 90% confidence intervals of observations. Similar proximity of predictions to observed scenarios was also noted for mean sizes of ice crystals. These microphysical properties are of great importance in radiation and aerosol-cloud interactions for determining the optical properties of clouds. Precipitation has also been predicted more accurately by the scheme for both cases especially for CLASIC. This further affirms the robustness of the model. Moreover, the radiation statistics were also simulated satisfactorily, with a model bias of less than $\pm 25\%$ for both top of the atmosphere and surface radiative fluxes. Downward and upward components of long- and short-wave radiations were predicted for both cases.

This scheme has been improved and upgraded, making it adaptable to a wide range of atmospheric science studies particularly investigations of aerosol-cloud interactions. This updated and rigorously validated aerosol-cloud model allows research of aerosol indirect effects and was used to investigate the different mechanisms of aerosol indirect effects particularly on glaciated clouds. This study was the first of its kind using such a robust, state-of-the-art microphysics scheme comprising a semi-prognostic aerosol component, encapsulating diverse aerosol species and explicitly treating their loadings and chemical compositions. The focus of part two of this paper is to investigate different and salient mechanisms by which changes in

aerosol fields, both in their number concentration and chemical composition, affect the optical properties of clouds. The main objectives of the study shall be to explore the cloud microphysical and dynamical mechanisms for glaciated cloud indirect effects on the mesoscale, focusing mainly on glaciation, thermodynamic and riming indirect effects (Lohmann and Feichter 2005) from anthropogenic soluble and solid aerosols. Important feedbacks associated with these indirect effects are investigated as well as quantifying their respective radiative forcings. This shall done by way of sensitivity tests.

Acknowledgement

The work was funded by an award to, and was directed by Vaughan T. J. Phillips (VTJP) from Office of Science (BER), US Department of Energy (DE-SC0002383, which later became DE-SC0007396). The authors are also grateful to the anonymous reviewers for their constructive criticism.

A. Microphysical Conversions

Symbol	Meaning
$\mathrm{Ac}(\mathrm{q}_g;\, \mathrm{q}_w \mid q_g)$	Riming of cloud liquid by graupel
$\mathrm{Ac}(\mathrm{q}_g;\, \mathrm{q}_i \mid q_g)$	Accretion of cloud ice by graupel
$\mathrm{Ac}(\mathrm{q}_g;\, \mathrm{q}_s \mid q_g)$	Accretion of snow by graupel
$\mathrm{Ac}(\mathrm{q}_g;\, \mathrm{q}_r \mid q_g)$	Accretion of rain by graupel
$\mathrm{Ac}(\mathrm{q}_g;\, \mathrm{q}_r \mid q_i)$	Accretion of cloud ice by rain
$\mathrm{Ac}(\mathrm{q}_g/\mathrm{q}_s;\, \mathrm{q}_s \mid q_r)$	Accr of snow by rain, to graupel or snow
$\mathrm{Ac}(\mathrm{q}_g/\mathrm{q}_s;\, \mathrm{q}_r \mid q_s)$	Accr of rain by snow, to graupel or snow
$\mathrm{Ac}(\mathrm{q}_r;\, \mathrm{q}_w \mid q_r)$	Accretion of cloud liquid by rain
$\mathrm{Ac}(\mathrm{q}_s;\, \mathrm{q}_w \mid q_s)$	Riming of cloud liquid by snow
$\mathrm{Ac}(\mathrm{q}_s;\, \mathrm{q}_i \mid q_s)$	Accretion of cloud ice by snow
$\mathrm{Ac}(\mathrm{q}_s;\, \mathrm{q}_w \mid q_i)$	Snow from cloud ice by riming

Table 3. *Microphysical conversion tendencies for mass mixing ratio (kg $kg^1 s^1$) (Sect. 2.2.5). The final species in each interaction is the first symbol within parentheses, while symbols after the semicolon denote the initial interacting species.*

References

Allen, G., et al., 2008: Aerosol and trace-gas measurements in the darwin area during the wet season. *Journal of Geophysical Research: Atmospheres (1984–2012)*, **113 (D6)**.

Benmoshe, N. and A. Khain, 2014: The effects of turbulence on the microphysics of mixed-phase deep convective clouds investigated with a 2-d cloud model with spectral bin microphysics. *Journal of Geophysical Research: Atmospheres*.

Berg, L. K., C. M. Berkowitz, J. C. Barnard, G. Senum, and S. R. Springston, 2009: Overview of the cumulus humilis aerosol processing study. *B. Am.Meteorol. Soc.*, **90 (11)**, 1653, doi:10.1175/2009BAMS2760.1.

Boucher, O. and D. Randall, 2013: Climate change 2013: The physical science basis. contribution of working group i to the fifth assessment report of the intergovernmental panel on climate change, (ipcc). *Cambridge University Press, Cambridge, United Kingdom and New York, NY, USA.*, **5th**.

Charlson, R., S. E. Schwartz, J. Hales, R. Cess, J. J. Coakley, H. JE., and H. DJ., 1992: Climate forcing by anthropogenic aerosols. *Science*, **255 (5043)**, 423–30.

Clark, T. L., 1974: A study of cloud phase parameterization using the gamma distribution. *J. Atmos. Sci*, **31**, 142–155.

Clarke, A. D., et al., 2004: Size distributions and mixtures of dust and black carbon aerosol in asian outflow: Physiochemistry and optical properties. *Journal of Geophysical Research: Atmospheres*, **109**, D15S09.

Ferrier, S. B., 1994: A double-moment multiple-phase four-class bulk ice scheme. part i: Description. *Journal of the Atmospheric Sciences*, **51 (2)**, 249–280.

Fridlind, A., A. Andrew, P. Jon, F. Paul, A. Hill, M. Greg, X. Shaocheng, and Z. Minghua, 2009: Arm/gcss/sparc twp-ice crm intercomparison study, tWP-ICE technical report.

Fridlind, A. M. and Co-authers, 2012: A comparison of twp-ice observational data with cloud-resolving model results. *J. Geophys. Res*, **117**, D05 204,, doi:10.1029/2011JD016595.

Gettelman, A., X. Liu, D. Barahona, D. Lohmann, and C. Chen, 2012: Climate impacts of ice nucleation. *Journal of Geophysical Research: Atmospheres*, **117 (D20)**, D20 201.

Haywood, J. and O. Boucher, 2000: Estimates of the direct and indirect radiative forcing due to tropospheric aerosols: A review. *Reviews of Geophysics*, **38 (4)**, 513–543.

Heymsfield, A., A. Bansemer, P. Field, S. Durden, J. Stith, J. Dye, W. Hall, and C. Grainger, 2002: Observations and parameterizations of particle size distributions in deep tropical cirrus and stratiform precipitating clouds: Results from in-situ observations in trmm field campaigns. *Journal of the Atmospheric Sciences*, **59**, 3457–3491.

Heymsfield, A., A. Bansemer, and C. Twohy, 2007a: Refinements to ice particle mass dimensional and terminal velocity relationships for ice clouds: Part 1: Temperature dependence. *Journal of the Atmospheric Sciences*, **64**, 1047–1067, doi:10.1175/JAS3890.1.

Hill, A. A. and S. Dobbie, 2008: The impact of aerosols on non-precipitating marine stratocumulus. ii: The semi-direct effect. *Quarterly Journal of the Royal Meteorological Society*, **134**, 1155–1165, doi:10.1002/qj.277.

Johnson, B., K. Shine, and P. Forster, 2004: The semi-direct aerosol effect: Impact of absorbing aerosols on marine stratocumulus. *Quarterly Journal of the Royal Meteorological Society*, **130 (599)**, 1407–1422.

Johnson, B. T., 2003: The semi-direct aerosol effect. Ph.D. thesis, The University of Reading.

Kajikawa, M. and A. J. Heymsfield, 1989: Aggregation of ice crystals in cirrus. *J. Atmos. Sci.*, **46**, 3108–3121, doi:http://dx.doi.org/10.1175/1520-0469(1989)046⟨3108:AOICIC⟩2.0.CO;2.

Kessler, E., 1969: On the distribution and continuity of water substance in atmospheric circulations. *Meteor. Monogr.*, **32**.

Khairoutdinov, M. and Y. Kogan, 2000: A new cloud physics parameterization in a large-eddy simulation model of marine stratocumulus. *American Meteorological Society*, **128**, 229–243.

Koch, D. and A. D. Genio, 2010: Black carbon semi-direct effects on cloud cover: review and synthesis. *Atmospheric Chemistry and Physics*, **10 (16)**, 7685–7696.

Kudzotsa, I., 2013: Mechanisms of aerosol indirect effects on glaciated clouds simulated numerically. Ph.D. thesis, University of Leeds, UK.

Liao, H. and J. H. Seinfeld, 1998: Effect of clouds on direct aerosol radiative forcing of climate. *Journal of Geophysical Research: Atmospheres (1984–2012)*, **103 (D4)**, 3781–3788.

Lim, K. S. S. and Y. S. Hong, 2010: Development of an effective double-moment cloud microphysics scheme with prognostic cloud condensation nuclei (ccn) for weather and climate models. *American Meteorological Society*, **138**, 1587–1612, doi:10.1175/2009MWR2968.1.

Lin, Y. L., R. D. Farley, and H. D. Orville, 1983: Bulk parameterization of the snow field in a cloud model. *Journal of climate applications: Meteorology*, **22**, 1065–1092.

Lohmann, U. and J. Feichter, 2001: Can the direct and semi-direct aerosol effect compete with the indirect effect on a global scale? *Geophysical Research Letters*, **28 (1)**, 159–161.

Lohmann, U. and J. Feichter, 2005: Global indirect aerosol effects: a review. *Atmospheric Chemistry and Physics*, **5 (3)**, 715–737, doi:10.5194/acp-5-715-2005, URL http://www.atmos-chem-phys.net/5/715/2005/.

Lohmann, U., P. Stier, C. Hoose, S. Ferrachat, S. Kloster, E. Roeckner, and J. Zhang, 2007: Cloud microphysics and aerosol indirect effects in the global climate model echam5-ham. *Atmospheric Chemistry and Physics*, **7 (13)**, 3425–3446.

MacPherson, J. and G. Isaac, 1977: Turbulent characteristics of some canadian cumulus clouds. *Journal of Applied Meteorology*, **16 (1)**, 81–90.

Mann, G., K. Carslaw, D. Spracklen, D. Ridley, P. Manktelow, M. Chipperfield, S. Pickering, and C. Johnson, 2010: Description and evaluation of glomap-mode: a modal global aerosol microphysics model for the ukca composition-climate model. *Geoscientific Model Development*, **3 (2)**, 519–551.

Matthias-Maser, S. and R. Jaenicke, 1995: The size distribution of primary biological aerosol particles with radii ¿ 0.2-m in an urban/rural influenced region. *Atmos. Res.*, **39 (4)**, 279–286.

May, P. T., J. H. Mather, V. Geraint, B. Keith N., J. Christian, M. Greg M., and M. Gerald G., 2008: The tropical warm pool international cloud experiment. *American Meteorological Society*, **89**, 629–645, doi:http://dx.doi.org/10.1175/BAMS-89-5-629.

McComiskey, A. and G. Feingold, 2012: The scale problem in quantifying aerosol indirect effects. *Atmospheric Chemistry and Physics*, **12 (2)**, 1031–1049.

Menon, S., A. D. Genio, D. Del Koch, and G. Tselioudis, 2002a: Gcm simulations of the aerosol indirect effect: Sensitivity to cloud parameterization and aerosol burden. *Journal of the Atmospheric Sciences*, **59 (3)**, 692 – 713, doi:10.1175/1520-0469(2002)059-0692:GSOTAI-2.0.CO;2.

Miller, M. A., 2007: Sgp cloud and land surface interaction campaign (clasic): Science and implementation plan. *DOE/SC-ARM-0703*.

Ming, Y., V. Ramaswamy, L. J. Donner, and V. T. J. Phillips, 2006: A new parameterization of cloud droplet activation applicable to general circulation models. *Journal of the atmospheric sciences*, **63**, 1348–1356.

Mitchell, D. L., 1994: A model predicting the evolution of ice particle size spectra and radiative properties of cirrus clouds. part i: Microphysics. *Journal of Atmospheric Sciences*, **51 (6)**, 797–816.

Mitchell, D. L. and W. P. Arnott, 1994: A model predicting the evolution of ice particle size spectra and radiative properties of cirrus clouds. part ii: Dependence of absorption and extinction on ice crystal morphology. *J. Atmos. Sci.*, **51**, 817–832.

Morrison, H. and W. W. Grabowski, 2011: Cloud-system resolving model simulations of aerosol indirect effects on tropical deep convection and its thermodynamic environment. *atmospheric chemistry and physics*, **11**, 10 503–10 523, doi:10.5194/1cp-11-10503-2011.

Murray, B. J., et al., 2010: Heterogeneous nucleation of ice particles on glassy aerosols under cirrus conditions. *Nature Geosci*, **3**, 233–237, doi:10.1038/ngeo817.

Musil, D. J., 1970: Computer modeling of hailstone growth in feeder clouds. *Journal of the Atmospheric Sciences*, **27 (3)**, 474–482.

Myhre, G., et al., 2009: Modelled radiative forcing of the direct aerosol effect with multi-observation evaluation. *Atmospheric Chemistry and Physics*, **9 (4)**, 1365–1392.

O'Donnell, D., K. Tsigaridis, and J. Feichter, 2011: Estimating the direct and indirect effects of secondary organic aerosols using echam5-ham. *Atmos. Chem. Phys.*, **11**, 8635–8659.

Petters, M. D. and S. M. Kreidenweis, 2007: A single parameter representation of hygroscopic growth and cloud condensation nucleus activity. *Atmospheric Chemistry and Physics*, **7 (8)**, 1961–1971, doi:10.5194/acp-7-1961-2007, URL http://www.atmos-chem-phys.net/7/1961/2007/.

Phillips, V., et al., 2005: Anvil glaciation in a deep cumulus updraught over florida simulated with the explicit microphysics model. i: Impact of various nucleation processes. *Quarterly Journal of the Royal Meteorological Society*, **131**, 2019–2046, doi:10.1256/qj.04.85.

Phillips, V. T., M. Formenton, A. Bansemer, I. Kudzotsa, and B. Lienert, 2015: A parameterization of sticking efficiency for collisions of snow and graupel with ice crystals: Theory and comparison with observations. *Journal of the*

Atmospheric Sciences.

Phillips, V. T. J., C. Andronache, B. C. E. Morris, D. C. Sands, A. Bansemer, A. Lauer, C. McNaughton, and C. Seman, 2009: Potential impacts from biological aerosols on ensembles of continental clouds simulated numerically. *Biogeosciences*, **6**, 987–1014.

Phillips, V. T. J., P. J. DeMott, and C. Andronache, 2008: An empirical parameterization of heterogeneous ice nucleation for multiple chemical species of aerosol. *Journal of the atmospheric sciences*, **65**, 2757–2783, doi:10.1175/2007JAS2546.1.

Phillips, V. T. J., P. J. Demott, C. Andronache, K. A. Pratti, and C. Twohy, 2013: Improvements to an empirical parameterization of heterogeneous ice nucleation and its comparison with observations. *J. Atmos. Sci.*, **70**, 378–409.

Phillips, V. T. J., L. J. Donner, and S. T. Garner, 2007: Nucleation processes in deep convection simulated by a cloud-system-resolving model with double-moment bulk microphysics. *Journal of the Atmospheric Sciences*, **64**, 738–761, doi:http://dx.doi.org/10.1175/JAS3869.1.

Pruppacher, H. R. and J. D. Klett, 1997: *Microphysics of clouds and precipitation*. Kluwer accademic publishers.

Pruppacher, H. R. and J. D. Klett, 2010: *Microphysics of Clouds and Precipitation*, Vol. 18. 2d ed., Reidel Publishing Company, 609 pp.

Reisner, J., R. M. Rasmussen, and R. T. Bruintjes, 1998: Explicit forecasting of supercooled liquid water in winter storms using the mm5 mesoscale model. *Quart. J. Roy. Meteor. Soc.*, **124**, 1071–1107.

Rogers, R. R. and M. K. Yau, 1991: *A short course in cloud physics*. 3d ed., Perganom.

Solomon, S., D. Qin, M. Manning, Z. Chen, M. Marquis, K. Averyt, M.Tignor, and H. M. (eds.), 2007: Climate change 2007: The physical science basis. contribution of working group i to the fourth assessment report of the intergovernmental panel on climate change, (ipcc). *Cambridge University Press, Cambridge, United Kingdom and New York, NY, USA.*, **4th**.

Spracklen, D., K. Pringle, K. Carslaw, M. Chipperfield, G. Mann, et al., 2005: A global off-line model of size-resolved aerosol microphysics: I. model development and prediction of aerosol properties. *Atmospheric Chemistry and Physics*, **5 (8)**, 2227–2252.

Thompson, G., R. M. Rasmussen, and K. Manning, 2004: Explicit forecasts of winter precipitation using an improved bulk microphysics scheme. part i: Description and sensitivity analysis. *American Meteorological Society*, **132**, 519–552.

Walko, R. L., W. R. Cotton, M. P. Meyers, and J. Y. Harrington, 1995: New rams cloud microphysics parameterization. part i: The single-moment scheme. *Atmos. Res*, **38**, 29–62.

